Available online at www.sciencedirect.com
ScienceDirect
Medical Image Analysis 12 (2008) 291–299
MEDICAL IMAGE ANALYSIS
www.elsevier.com/locate/media

Robust parametrization of brain surface meshes

Frithjof Kruggel *

Department of Biomedical Engineering, University of California, 204 Rockwell Engineering Center, Irvine, CA 92697-2755, USA

Received 15 June 2007; received in revised form 13 October 2007; accepted 28 November 2007
Available online 23 December 2007

Abstract

Complex shapes – such as the surface of the human brain – may be represented and analyzed in frequency space by means of a spherical harmonics transformation. A key step of the processing chain is introducing a suitable parametrization of the triangular mesh representing the brain surface. This problem corresponds to mapping a surface of topological genus zero on a unit sphere. An algorithm is described that produces an optimal combination of an area- and angle-preserving mapping. A multi-resolution scheme provides the robustness required to map the highly detailed and convoluted brain surface. More than 1000 datasets were successfully processed by this mature and robust approach.

Keywords: Magnetic resonance imaging; Brain surface; Surface parametrization; Spherical harmonics transformation

1. Introduction

It is a well-known fact in neuroanatomy that structural variants of the brain exist, some of which have to be considered as pathologic (e.g., macrogyria or microgyria) or abnormal (e.g., callosal agenesis) – but even normal brains exhibit a considerable variability. Brain shapes do not necessarily form a continuum in some descriptor space, but may cluster due to pre-determined genetical factors or acquired diseases.

An interesting approach for describing shapes is provided via a spherical harmonics transformation (SHT) that may be understood as a "Fourier transform on a sphere". Any surface of genus zero can be transformed into frequency space using a linear combination of basic shapes, and the resulting parameters of the shape spectrum can be used as a parsimonous shape description. The shape space spanned by spherical haramonic basis functions is orthogonal, and readily offers a metric for comparing and classifying shapes (Brechbühler et al., 1996; Funkhouser et al., 2003; Gerig et al., 2001; Shen et al., 2004).

Implementing this apparently attractive approach poses difficult problems when highly convoluted objects with detailed structures are under study, such as the surface of the human brain. First, the brain's surface must be extracted from magnetic resonance (MR) imaging data of the human head, usually as a triangular mesh. This is considered a complex, but well developed methodology in medical image processing (Kruggel, 2005). The "tricky" part is to ensure that the surface has a topological genus of zero (Fischl et al., 2001; Han et al., 2002, 2003; Shattuck and Leahy, 2001) and is free of self-intersections (Gumhold et al., 2003; Park et al., 2001).

For computing a SHT, a parameterization of the surface must be introduced which corresponds to mapping it onto a (unit) sphere. Such a mapping can be either angle- *or* area-preserving but not *isometric* (both) – which is most desirable because all properties of the surface are represented in the parameter domain. Finding an angle-preserving mapping yields an *almost unique* solution: all mappings form a so-called Möbius group (Gu et al., 2004). Equiareal mappings are substantially different because from the point of view of uniqueness there are many more of them. In order to find a well-behaved mapping we need to aim for area-preservation with some minimization of angular

* Tel.: +1 949 824 3729; fax: +1 949 824 1727.
E-mail address: fkruggel@uci.edu

1361-8415/$ - see front matter © 2007 Elsevier B.V. All rights reserved.
doi:10.1016/j.media.2007.11.001

distortion. For a comprehensive discussion of current mapping techniques and their foundation in differential geometry, refer to the survey by Floater and Hormann (2005).

Several approaches were proposed for parametrization of brain surface meshes: The conformal mapping procedure proposed by Angenent et al. (1999) first maps the input mesh onto a plane using the Laplace–Beltrami operator and then uses a stereographic projection to map to the sphere. It requires an (arbitrary) selection of a "pole" for the projection and an (arbitrary) splitting of the sphere. So the area distortion of the final map depends on the selection of the pole and the split. This method is very fast, but may fail due to numerical instabilities when solving the underlying partial differential equation as a large sparse linear equation system. Tosun et al. (2004) built upon this procedure and add a Möbius transformation to minimize area distortion of the final mapping. Before mapping, a surface is inflated (flattened) to obtain a more regular mesh structure. This flattening reduces the curvature scale and improves the numerical stability of the equation system. However, metric properties are optimized for the inflated surface, so the relation of angles, distances and areas for the brain mesh vs. the spherical map are unspecified. Gu et al. (2004) later proposed an iterative method for generating a conformal map by minimizing the harmonic energy. This approach may generate triangle flips when the mesh has obtuse angles, and they suggest local remeshing as a preprocessing step to ensure that all angles are acute. Hurdal and Stephenson (2004) used the fact that classical analytic functions can be approximated using circle packing, and proposed a mapping procedure based on circle packing. However, this approach considers connectivity only and does not preserve metric properties. Finally, Fischl et al. (1999) described a mapping algorithm that minimizes metric distortion and unfolds sulci based on a signed area term. An implementation is widely available in the FreeSurfer software package. In comparison, metric surface properties are preserved best by this algorithm (Ju et al., 2005), however, the solution is not unique (Floater and Hormann, 2005), and the method is computationally very demanding.

These drawbacks of current mapping approaches triggered the development of a mapping algorithm that is robust enough to handle large, convoluted brain surface meshes consisting of up to 500,000 triangles. It provides an optimum of angle- and area-preservation that comes close to isometry which is most desirable for a parametrization that is used for a SHT. Preprocessing is not required (e.g., selecting a pole, inflation, or remeshing for acute angles). More than 1000 hemispheres were successfully processed, so we consider our approach as mature and robust.

2. Algorithms

Three steps are required to achieve a shape description by SHT: (1) extraction of the surface from imaging data as a triangle mesh, (2) parametrization of the mesh by spherical mapping, and (3) computation of the SHT. We focus on the description of an algorithm to perform step (2), but outline steps (1) and (3) for completeness.

2.1. Surface generation

Any method may be used to obtain a triangulated mesh representing the grey/white matter (GM/WM) interface. We briefly outline our procedure. T_1-weighted volumetric MR images were aligned with the stereotaxic coordinate system and interpolated to an isotropic voxel size of 1mm using a fourth-order b-spline method. Data were corrected for intensity inhomogeneities by a fuzzy segmentation approach using three classes (Pham and Prince, 1999), roughly corresponding to background and cerebrospinal fluid (class 0), GM, muscles and connective tissue (class 1), WM and fat (class 2). A mask for the brain's WM was extracted from intensity class 2 by removing the outer hulls of the brain and cutting the brainstem by an axial plane 15 mm below the posterior commissure. The biggest c18-connected component (Toriwaki and Yonekura, 2002) is retained as the raw WM segmentation of the cerebrum. The resulting raw WM segmentation was edited to have a topological genus of zero (Shattuck and Leahy, 2001). A triangulated surface was generated from the binary white matter segmentation using a variant of the "Marching Cubes" algorithm that preserves the original topology (Cignoni et al., 2000). An improved representation of the GM/WM interface was obtained by treating the initial mesh as a deformable model (Kruggel, 2005). Finally, we split the surface mesh at the mid-sagittal plane to yield separate meshes representing the GM/WM interface of each hemisphere.

2.2. Surface parametrization

A parametric surface is defined by an one-to-one mapping $\phi : \Omega \mapsto \mathbf{R}^3$, with $\Omega \subset \mathbf{R}^2$ the parameter domain, and we denote ϕ a parameterization of the surface. In our case, this parameter domain are the longitude and latitude (u, v) of the unit sphere. More specifically, a parameterization of a surface S that has a triangulation is sought:

$$\mathscr{M} = \{[1 \ldots n], \mathscr{T}, (s_i)_{i=1\ldots n}\}, \tag{1}$$

where $[1 \ldots n]$ denotes vertices at positions s_i and $\mathscr{T}$ their set of corresponding triangles $\Delta_{\mathscr{M}}$. We require that the parameterization is piecewise linear so that ϕ maps vertices and triangles of $\mathscr{M}$ onto vertices and triangles of the spherical triangulation $\mathscr{M}'$. The parameterization is found by minimizing a suitable error metric for the mapping over the parameter domain. As a result, we find parameters (u_i, v_i) for each vertex s_i of the surface mesh.

Metric properties of S are characterized by its first fundamental form (for a thorough derivation, refer to Kreyzsig, 1991):

$$\mathbf{I}_\phi = \nabla^{\mathrm{T}}\phi \cdot \nabla\phi = \begin{pmatrix} a & b \\ b & d \end{pmatrix}, \quad \text{with } a = \left\|\frac{\partial\phi}{\partial u}\right\|^2,$$
$$b = \left\langle \frac{\partial\phi}{\partial u}, \frac{\partial\phi}{\partial v} \right\rangle, \; c = \left\|\frac{\partial\phi}{\partial v}\right\|^2. \tag{2}$$

A parametrization ϕ is called *isometric* if $\mathbf{I}_\phi = I_2$, where I_2 corresponds to the 2×2 identity matrix. Isometric parametrizations only exist for surfaces with zero Gaussian curvature: only developable surfaces (e.g., planar, cylindrical or conical surfaces) can be parametrized without distortion.

A conformal (angle-preserving) parametrization requires that $\mathbf{I}_\phi(\omega) = c(\omega)I_2$ for every $\omega \in \Omega$, where c corresponds to the so-called conformal factor (Gu et al., 2004). Thus, the conformality of a parametrization can be expressed as the ratio of both singular values σ_1/σ_2 of $\mathbf{I}_\phi$. This ratio is equal to one for all mappings that do not deform shape. For an area-preserving parametrization, $\det(\mathbf{I}_\phi) = 1$, or $\sigma_1\sigma_2 = 1$ (Floater and Hormann, 2005).

2.2.1. Error metric

A suitable error metric for obtaining an (almost) isometric parametrization was proposed by Degener et al. (2003). Conditions for conformality and area-preservation should yield values close to one. The function $f(x) = x + \frac{1}{x}$ is convex, has its minimum at $x = 1$, and grows to infinity for $x \to 0$ and $x \to \infty$ (Hormann, 2001).

Substituting x by the ratio of the area of $\Delta_{\mathcal{M}}$ and the mapped triangle $\Delta_{\mathcal{M}'}$ defines the error term E_{area} for area-preservation:

$$E_{\text{area}} = \frac{\text{area}(\Delta_{\mathcal{M}})}{\text{area}(\Delta'_{\mathcal{M}})} + \frac{\text{area}(\Delta'_{\mathcal{M}})}{\text{area}(\Delta_{\mathcal{M}})} - 2. \tag{3}$$

Substituting x by the ratio σ_1/σ_2 yields an error term E_{angle} for angle preservation. Referring to the notation of Fig. 1, this term is given by:

$$E_{\text{angle}} = \frac{\cot\alpha|a|^2 + \cot\beta|b|^2 + \cot\gamma|c|^2}{2\text{area}(\Delta_{\mathcal{M}})}. \tag{4}$$

For details of the derivation of this term, refer to (Hormann, 2001; Pinkall and Polthier, 1993). Finally, the total distortion error of the map is

$$E_\phi = \sum_{\Delta\in\mathcal{T}} E_\Delta = \sum_{\Delta\in\mathcal{T}} E_{\text{angle}}(E_{\text{area}})^\rho \text{area}(\Delta_{\mathcal{M}'}), \tag{5}$$

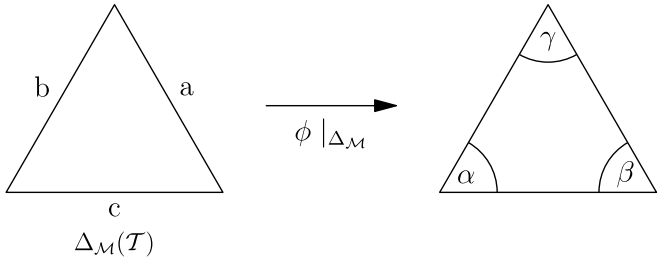

Fig. 1. Graphical explanation of the variables in the error function Eqs. (3) and (4).

where ρ varies between 0 and ∞ and controls the relative importance of angle and area-preservation (Degener et al., 2003).

2.2.2. Optimization

The coordinates (u_i, v_i) of vertex i affect only those E_Δ for which i is incident with Δ. Thus, only the partial error sum in the 1-ring (star) neighborhood of vertex i $E_i = \sum_{\Delta\in 1\text{-ring}(i)} E_\Delta$ is influenced by (u_i, v_i).

Given an initial configuration $(u_i, v_i)_{i=1\ldots n}$, first all vertices are ordered by their error E_i. Then, each vertex i is optimized in (u_i, v_i). The Simplex algorithm is used to solve this 2-parameter non-linear optimization problem (Press et al., 1999). The solution must be checked that (u_i, v_i) lies within the kernel of its 1-ring, so that triangles do not fold over. Minimizing E_i decreases E_ϕ in each step, so the algorithm is guaranteed to converge to a (local) minimum. We assume convergence if the change in E_ϕ falls below a predefined bound.

An initial configuration can be obtained by projecting vertices s_i to a position s'_i on the unit sphere, and by minimizing the distance of s'_i to all its adjacent vertices s'_j in the 1-ring:

$$s'_i = s'_i + \tau \sum_{j\in 1\text{-ring}(i)} |s'_j - s'_i|^2 \quad \text{with } \tau \in [0.10, 0.16]. \tag{6}$$

This process is iterated until all folded-over configurations are resolved.

2.2.3. Introducing robustness

For simple surfaces (i.e., a cube), mesh sizes of less than 50,000 triangles, and for $\rho = 0$, the algorithm above converges quickly. For complex surfaces (i.e., of a brain), larger meshes, and other settings of ρ, a multi-resolution scheme is employed. For surfaces with a small number of triangles, finding a solution (close) to the optimal one is more likely. The solution is propagated to the next more complex level, optimized again until a solution at the original resolution level is found.

The triangulated surface is subsampled by edge contraction. We basically use the iterative edge contraction method proposed by Garland and Heckbert (1999). By contracting an edge uv to form vertex w, both adjacent triangles can be removed (see Fig. 2). The position of the new contraction vertex w is determined by minimizing the so-called quadric error metric $Q_t(w) = \text{dist}(t, w)^2$ that is defined as the squared distance of w to the plane that contains triangle t. The edge contraction that introduces the lowest quadric error is considered first for removal. Subsampling an orientable 2-manifold closed surface of genus zero ultimatively leads to a tetrahedron. However, the original formulation of the algorithm neither preserved topology nor avoided self-intersections. We have to keep a topological genus of zero for the surface to preserve homotopy with a sphere. A self-intersection may result in a non-orientable surface in a subsequent simplification

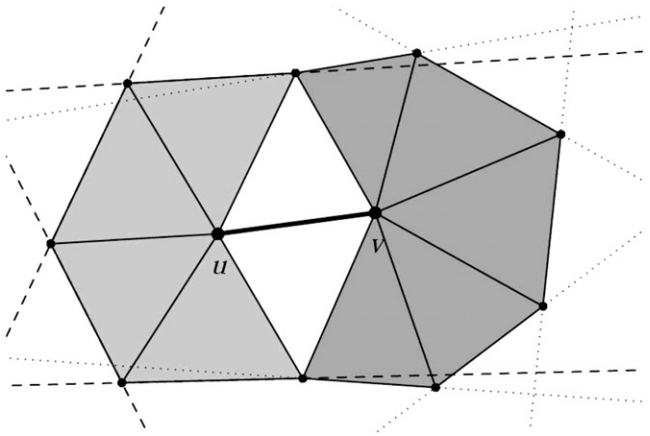

Fig. 2. Mesh simplification: by contracting the edge uv both adjacent triangles can be removed.

step. The next section describes how these constraints are imposed.

The sequence of changes (vertex/edge/triangle removal) is recorded and "played back" for propagating a solution onto the next resolution level. Typically, a subsampling factor $f = [1.2 \ldots 2.0]$ is used between levels. For our problem, starting at a lowest resolution level of 1000–5000 triangles is sufficient. In Fig. 3, surfaces at five resolution levels (50,000, 25,000, 12,500, 6250, 3125, 1623 triangles) and their corresponding spherical mapping are shown. Longitude and latitude of vertices at the highest resolution level serve as the parameterization of the input (brain) surface.

2.2.4. Constrained mesh simplification

Introducing a topology constraint is straightforward: if an edge contraction would change the genus, it is not performed. Remember that the genus g of a triangulated surface mesh is given by:

$$g = 1 - (n_v - n_e + n_f)/2,$$

where n_v corresponds to the number of vertices, n_e is the number of edges, and n_f is the number of faces. Note that we have to ensure that this mesh consists of a single connected component.

The formalism for avoiding self-intersections is rather involved: instead of just testing for self-intersections around the new vertex w after contraction, we need to check for intersections along the contraction paths uw and vw. Denote x and y as other vertices that are edge-connected to u or v. Then, the following tests are necessary for path uw (and vw, in parentheses) (Gumhold et al., 2003):

1. A triangle–edge intersection test between the contraction path $uw(vw)$ and all triangles in the local neighborhood that do not include vertex $u(v)$.
2. A edge–triangle intersection test between the triangle formed by $uw(vw)$ and any edge $ux(vx)$ with all edges in the local neighborhood that do not include vertices $u(v)$ and x.
3. A vertex-in-tetrahedron test between the tetrahedron formed by $uw(vw)$ and any triangle $uxy(vxy)$ with all vertices in the local neighborhood except $u, x, y(v, x, y)$.
4. A triangle–edge intersection test between the triangle uvw with all edges in the local neighborhood that do not include vertices u and v.
5. A vertex-in-tetrahedron test between the tetrahedron formed by $uw(vw)$ and any triangle uvx with all vertices in the local neighborhood except u, v, w, x.
6. A edge–triangle intersection test between the triangle uvw and any edge $ux(vx)$ in the local neighborhood except $u(v)$ as intersection point.
7. A edge–triangle intersection test between the edge vw and all triangles $uxy(vxy)$ in the local neighborhood.
8. A triangle–triangle intersection test between (a) all triangles formed by edge uw and any edge ux and (b) all triangles formed by edge vw and any edge vy.

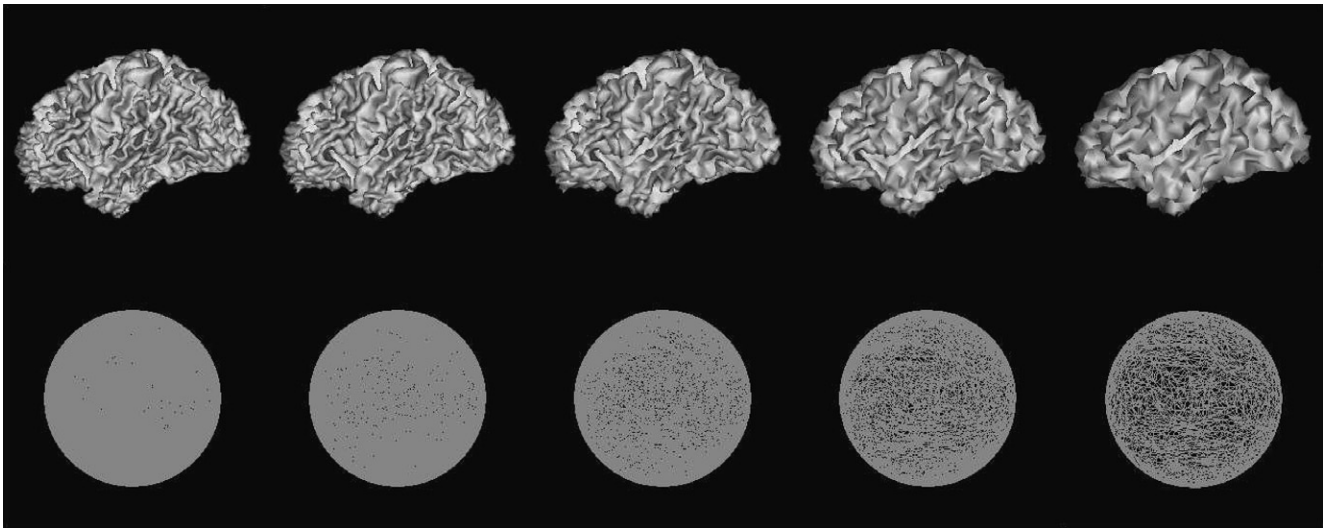

Fig. 3. Hemispheric surfaces at five resolution levels (50,000, 25,000, 12,500, 6250, 3125, 1623 triangles) and their corresponding spherical mapping.

If one of these tests indicates an intersection, the edge contraction is not performed. In order to quickly find primitives in the local neighborhood, a bounding box for primitive type I is computed and all primitives type II that intersect with the bounding box are included in the test. As an example, Algorithm 1 outlines test #2:

Algorithm 1. Triangle–edge intersection test

```
make a list l_t of all triangles t that contain the edge ux and
vertex w
compute the bounding box b enclosing all triangles l_t
make a list l_e of all edges e that intersect with the bound-
ing box b
for all t ∈ l_t do
   for all e ∈ l_e do
      if u,x are not vertices in e then
         if e and t intersect then
            return true
         end
      end
   end
end
return false
```

In order to quickly find all triangles in the bounding box, we use a spatial cache. The space enclosed by the surface mesh is divided into a regular grid of cells. For each cell, we maintain a list of all vertices, edges, and triangles partially or completely contained in the cell. The grid spacing is set to the average edge length. Note that the spatial cache must be updated after each successful edge contraction. Simplification of a triangular mesh of genus zero will ultimatively yield a tetrahedron. This fact can be used to test the correctness of the implementation.

2.3. Computation of the SHT coefficients

A SHT of degree $l_{\max}$ has $p = (l_{\max}+1)^2$ functions (Press et al., 1999). Given $(s_i, u_i, v_i)_{i=1\ldots n}$ points on the surface and their parameterization, we can assemble a $n \times p$ matrix B of complex-valued spherical harmonics $b_{i,j} = Y_l^m(u_i, v_i)$, where $j(l,m) = l^2 + l + m$, and a $n \times 3$ matrix $X = (s_i)^{\mathrm{T}}_{i=1\ldots n}$ of the spatial coordinates. Typically, $p \ll n$, so the $p \times 3$ coefficient matrix C with row entries $(c_l^m)^x, (c_l^m)^y, (c_l^m)^z$ is determined by least squares estimation:

$$C = (B^{\mathrm{T}}B)^{-1} B^{\mathrm{T}}X \tag{7}$$

To solve this large equation system on standard workstations, $B^{\mathrm{T}}B$ and $B^{\mathrm{T}}X$ are computed "on the fly". The surface approximation can be computed from these coefficients by the inverse transformation:

$$\hat{s}_i^{(t)}(u_i, v_i) = \sum_{l=0}^{l_{\max}} \sum_{m=-l}^{l} (c_l^m)^{(t)} Y_l^m(u, v) \quad t = \{x, y, z\}, \tag{8}$$

The distance $|\hat{s}_i - s_i|$ is a measure for the goodness-of-fit or reconstruction error.

3. Experiments

We used a database of 513 MRI brain datasets of healthy volunteers aged between 16 and 70 years (Kruggel,

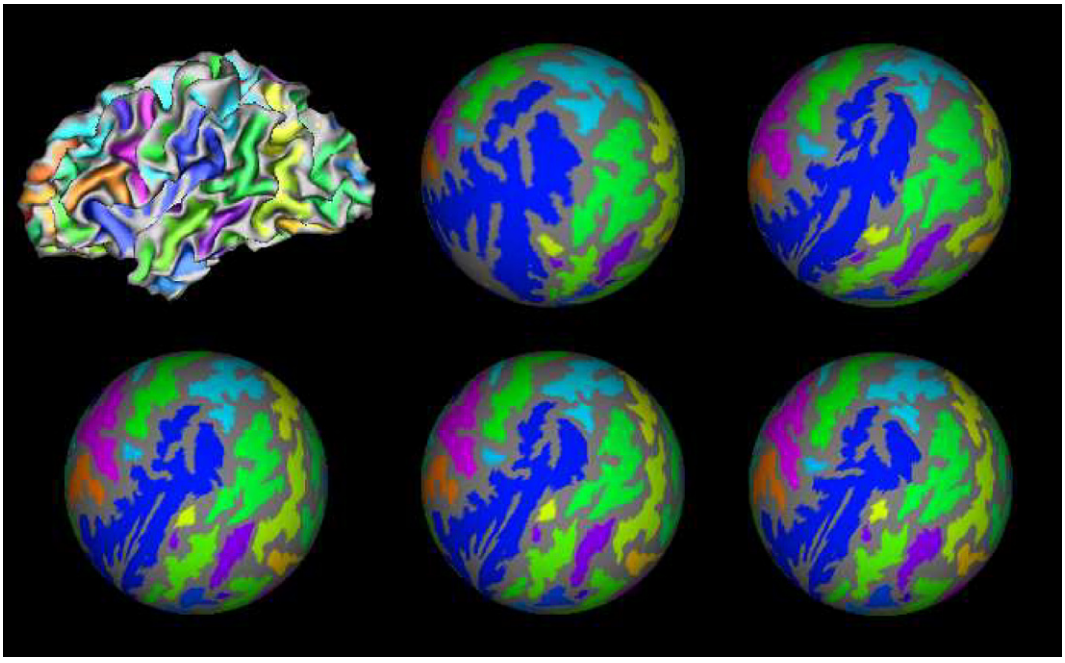

Fig. 4. Lateral view onto a WM surface of a left brain hemisphere (top left, 50,000 triangles), where sulcal substructures are color-coded. Subsequent images show the corresponding spherical mapping, for different settings of ρ: 0.0, 0.5, 1.0, 1.5, and 2.0.

2006). MR imaging was performed on a Bruker 3T Medspec 100 system, equipped with a bird cage quadrature coil. T_1-weighted images were acquired using a 3D modified driven equilibrium Fourier transform (MDEFT) protocol: field-of-view $220 \times 220 \times 192$ mm, matrix 256×256, TR = 1.3 s, TE = 10 ms, 128 sagittal slices, voxel size 0.9×0.9 mm, 1.5 mm slice thickness, scanning time 15 min.

Surfaces representing the GM/WM interface were computed from all datasets (a total of 1026 hemispheres), and were visually inspected for anatomical correctness. Note that these triangulated meshes were generated from interpolated datasets with isotropic voxel dimensions of 1 mm. All surfaces were successfully processed by the mapping algorithm with settings $\rho = 1, f = 1.3$. The processing time was about 20 min for the mapping and 15 min for the transformation on a standard workstation (AMD64, 2.4 GHz processor, Linux 2.6.15 operating system, 2 GB RAM).

Neurobiological results will be reported in a separate publication, we merely focus on evaluating technical aspects of the mapping algorithm here.

The first experiment demonstrates the influence of the mapping parameter ρ, which shifts properties of the algorithm from angle to area-preservation. This is depicted in Fig. 4: Sulci in an example hemisphere were color-coded and mapped with settings of ρ between 0 and 2. The relative change in shape and size of the mapped sulci is impressive.

In the next experiment, we studied the distribution of differences in angles, edge lengths and triangle areas induced by the mapping in dependence of ρ. Results for $\rho = \{0.0, 0.7, 1.0, 2.0\}$ are shown in Fig. 5. For $\rho = 0$, the method is angle-preserving *alone* due to the first term of the error function (top, red curve), but the error distribution of edge lengths (middle) and area (below) is broad. Increasing ρ to non-zero values introduces the preservation of edge lengths and areas while preserving angles, albeit at an increasing variance of the angle error with increasing ρ. Choosing $\rho = 1.0$ results in an optimal compromise between angle and area-preservation.

To demonstrate the robustness of this parametrization approach, we studied the error distributions in all 1026 hemispheres that were mapped using the same parameter setting ($\rho = 1, f = 1.3$). The mean and standard error of the error distributions in this sample are shown in Fig. 6, and correspond to the example graph from Fig. 5 (black line for $\rho = 1.0$).

The higher the degree $l_{\max}$ of this decomposition, the more detail is preserved, yielding a coarse-to-fine description with increasing number of parameters. We computed the reconstruction error (Fig. 7), color-coded on the GM/WM surface, depending on $l_{\max}$ for $\rho = 1.0$, and $l_{\max} = 5$ (top left), 15 (top right), 25 (bottom left), 35 (bottom right). The color scale runs from blue (0 mm) to red ($\geqslant 4$ mm).

Finally, we were interested in the average reconstruction error of the GM/WM interface as a function of the maxi-

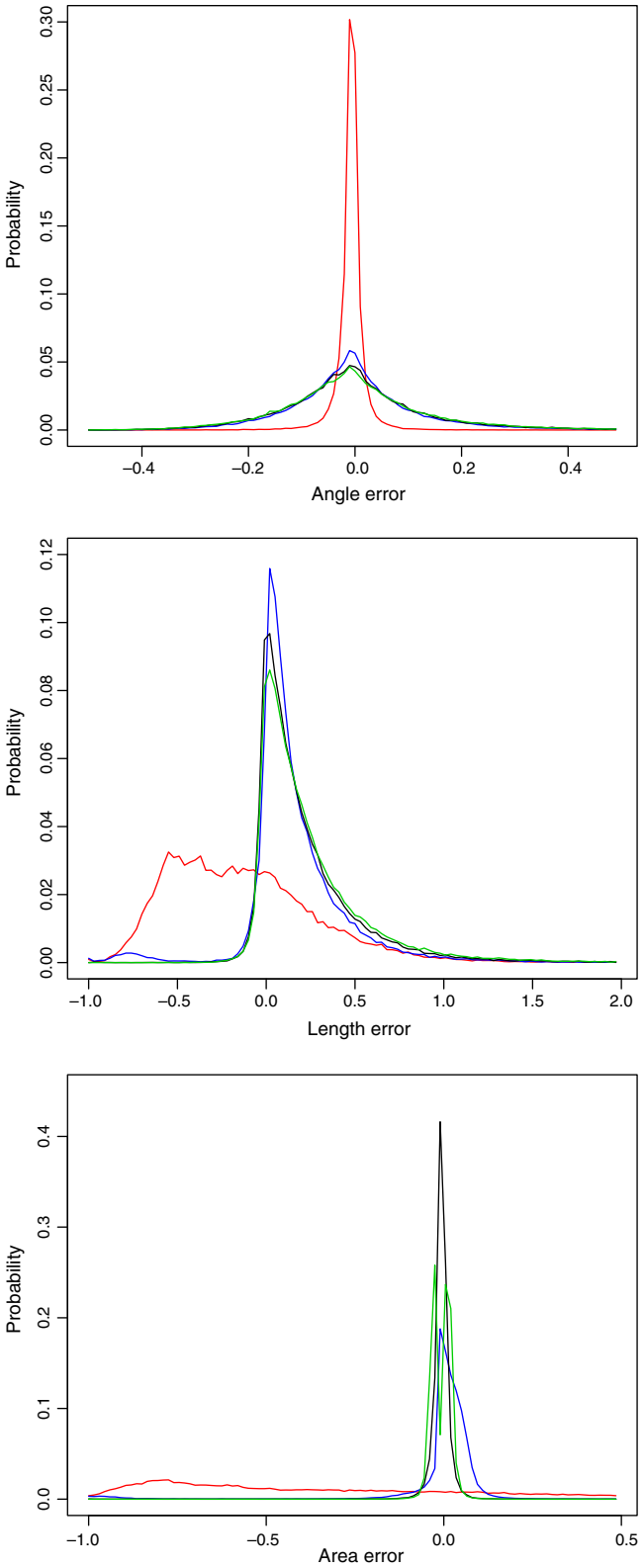

Fig. 5. Difference (as $v_{\text{map}}/v_{\text{true}} - 1$) for angles ($\alpha, \beta, \gamma$, top), edge lengths ($a, b, c$, middle), and areas A (below). Colors denote different settings of ρ: 0.0 (red), 0.7 (blue), 1.0 (black), and 2.0 (green). For $\rho = 0$, the method is angle-preserving *alone* due to the first term of the error function. Increasing ρ to non-zero values introduces the preservation of edge lengths and areas while preserving angles, albeit at an increasing variance of the angle error with increasing ρ.

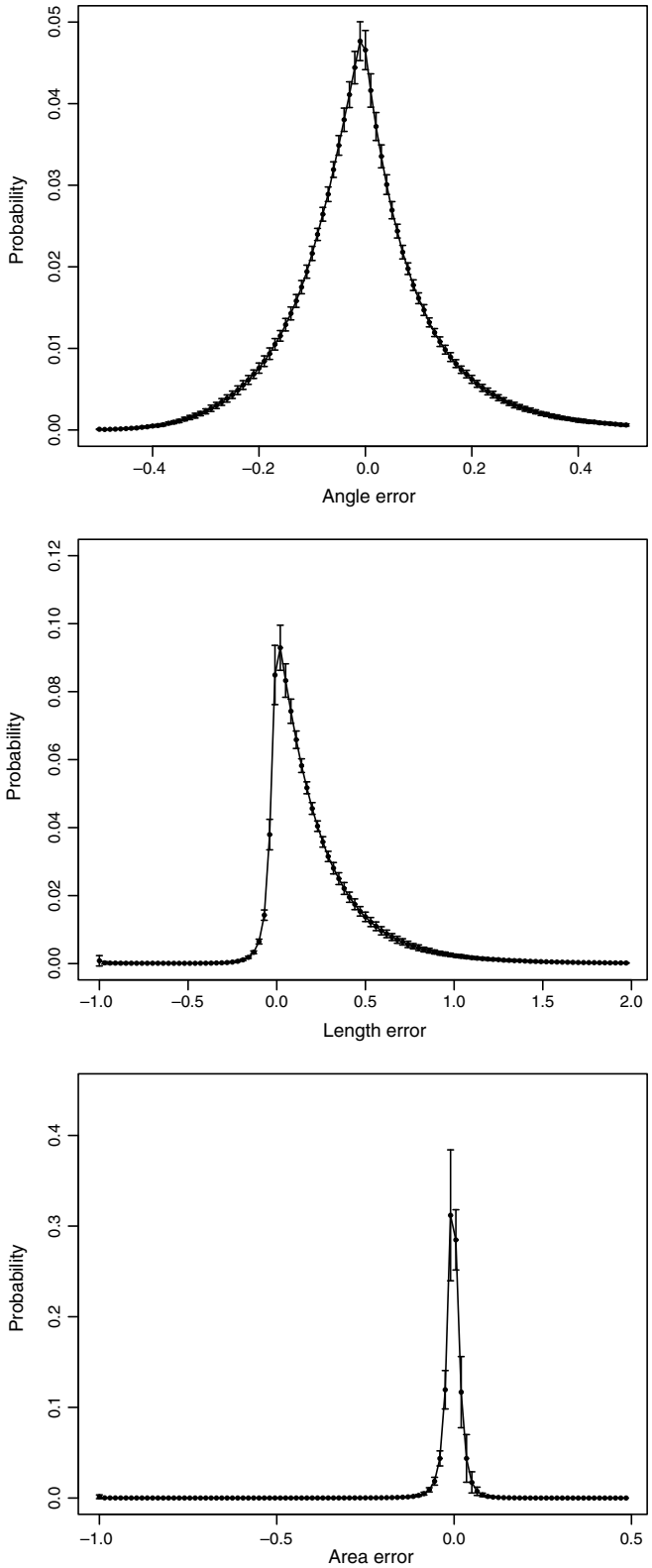

Fig. 6. Difference (as $v_{map}/v_{true} - 1$) for angles $(\alpha, \beta, \gamma, \text{top})$, edge lengths $(a, b, c$, middle), and areas A (below) for $\rho = 1$. Shown are the mean ($\pm$ standard error) of the error distribution obtained from processing the whole database of 1026 hemispheres. Compare results with Fig. 5 for $\rho = 1.0$ (black line).

mum SHT degree l_{max} and varying settings of ρ (circles: $\rho = 0.0$, triangles: $\rho = 1.0$, crosses: $\rho = 2.0$) (Fig. 8). To achieve a surface error that is in the order of the image resolution, $l_{max} \geqslant 30$ is required. Note that using an area-preserving mapping *always* yields a better reconstruction resp. to a lower l_{max}. Again, choosing $\rho = 1.0$ is optimal. For our problem, choosing an area-preserving mapping requires 35% less coefficients to achieve the same reconstruction error.

4. Discussion

The advantages of the proposed mapping algorithm are: (a) It is robust enough to handle large, highly convoluted meshes such as brain surfaces, and was tested with mesh sizes of up to 500,000 triangles. (b) By introducing an error metric that includes terms for area and angle-preservation, we achieve a mapping that comes close to isometry. (c) Compared with an angle-preserving mapping, substantially less coefficients are required to represent the brain surface with same reconstruction error.

Our procedure has two parameters. The exponent ρ in the error function weights terms regarding angle- and area-preserving properties of the mapping. Our evaluation demonstrates that introducing area-preservation by increasing ρ reduces the error on edge lengths and triangle areas, while the average angle error does not change noticably. Thus, increasing ρ leads to a more isotropic map - a very desirable feature. When mapping brain surfaces and aiming at a good compromise between area- and angle-preservation, we found that choosing ρ is not critical in the interval [1, 3], with an optimum at $\rho = 1$. Values beyond 3 did not influence results noticably. The setting of ρ influences the optimization: As discussed in the introduction, angle-preserving mappings have a unique optimum (up to a Möbius transformation), so for $\rho = 0$, a fast convergence is achieved, and less (or even no) multiresolution levels are required. Increasing ρ slows down convergence, and more more multiresolution levels are necessary to avoid suboptimal solutions.

The multiresolution approach increases the robustness of the algorithm. Besides the setting of ρ, the choice of the second parameter, the subsampling factor f is related to the convolutedness of the surface. For simple surfaces (e.g., similar to a cube or a sphere), a single level is sufficient. Values of f close to 1 increase the number of resolution levels (and thus, the computation time), but increase the likeliness of finding an optimal solution. For our mapping problem, values in the interval [1.3, 1.8] (corresponding to 30-7 levels) were sufficient. We processed all 1026 hemispheres with the same parameters $\rho = 1, f = 1.3$.

We would like to emphasize that the mesh simplification scheme described here is useful beyond this application. Most algorithms developed for computer graphics optimize on speed, and minimize on surface or volume error (Cignoni et al., 1998). This application (and similar problems in medical imaging) require in addition that the topology of the original mesh is preserved. As demonstrated, a topology constraint is easily integrated with

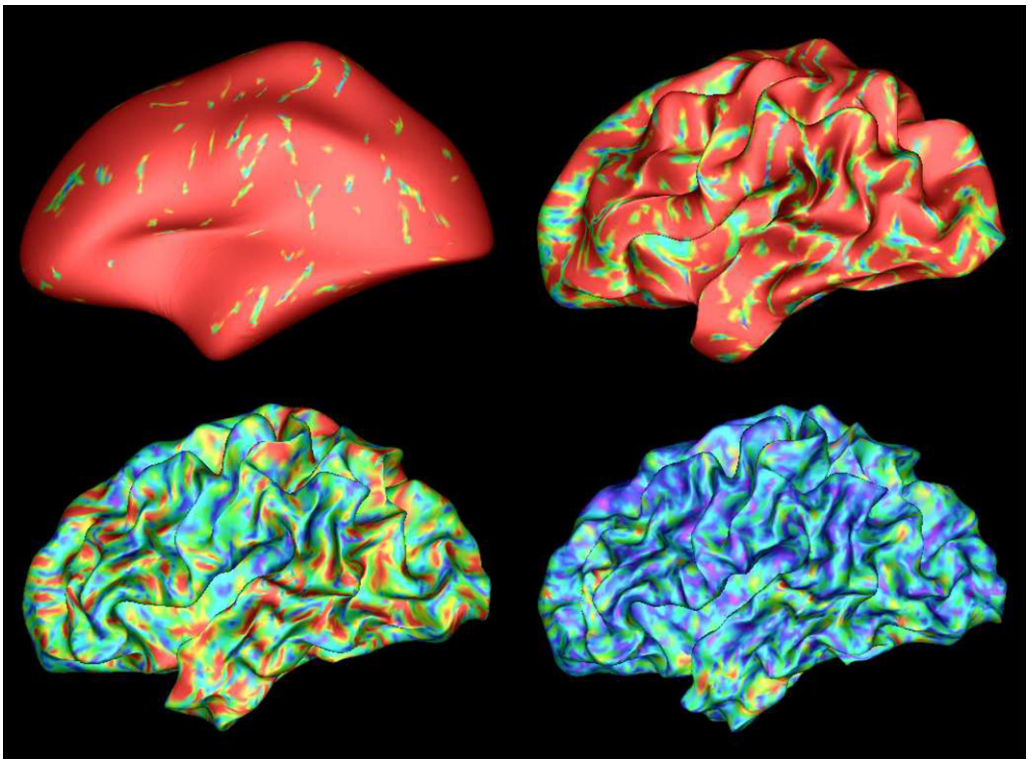

Fig. 7. Reconstruction error color-coded on the GM/WM surface depending on $l_{max} = 5$ (top left), 15 (top right), 25 (bottom left), 35 (bottom right). The color scale runs from blue (0 mm) to red ($\geqslant$4 mm).

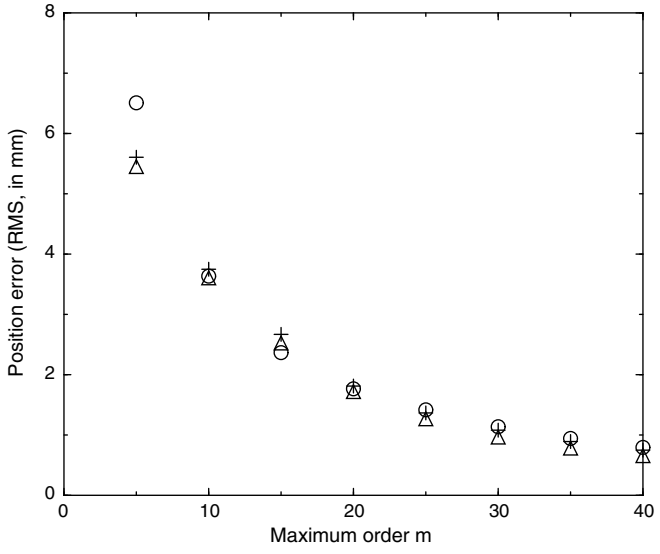

Fig. 8. Average reconstruction error of the GM/WM interface as a function of the maximum SHT degree l_{max} and varying settings of ρ (circles: $\rho = 0.0$, triangles: $\rho = 1.0$, crosses: $\rho = 2.0$).

mesh simplification. Most simplification schemes do not prevent the formation of self-intersections that are likely when simplifying highly convoluted surface meshes as encountered here. While self-intersecting surfaces are obviously anatomically invalid, a subsequent edge contraction step close to the intersection may lead to a non-orientable surface, and thus, to an invalid input for our mapping algorithm. So both constraints are indispensible for this algorithm, and are most likely required for similar applications in medical image analysis.

Our primary motivation for introducing a surface parametrization is obtaining a parsiomonous shape description of the brain surface via a SHT for further statistical analysis between gender and across age. Note that the obtained maps may be used for identifying sulci and gyri of the neocortical surface by matching surface features across subjects (or with an atlas).

Although we studied the mapping of brain surfaces exclusively here, it is well understood that our algorithm is applicable to any triangulated surface of genus zero, and thus, offers a general route for describing complex shapes by SHT coefficients. We would like to emphasize that this approach offers a range of general applications, notably in biomedical imaging and engineering:

- Shape representation: SHT allows a global, coarse-to-fine description of a complex surface.
- Shape analysis: Coefficients are suitable for statistical analysis, such as a classification of brain shapes. The area-preserving property allows quantitative comparisons of subregions across objects.
- Shape modeling: Models may be reconstructed to represent a smoothed version of the initial surface, or a "mean shape" from a set, i.e., for modeling tissue replacements.

- Information compression: Comparing storage requirements for the initial WM surface and the SHT coefficient array ($l_{max} = 35$, average error <0.7 mm), a compression ratio of 1:580 is achieved.
- Shape retrieval: The sparse set of coefficients, and the coarse-to-fine representation are interesting options for building shape databases and the design of efficient similarity metrics and search strategies.

Our primary goal is to describe the brain's shape by a sparse set of parameters. We will analyze shape differences across age and between gender, and derive statistics to detect significant shape differences.

Acknowledgement

This research was partially supported by Interdisziplinäres Zentrum für Klinische Forschung (IZKF) at the University of Leipzig (Project C15), Germany. Datasets were kindly provided by the MPI of Human and Cognitive Brain Science, Leipzig.

References

Angenent, S., Haker, S., Tannenbaum, A., Kikinis, R., 1999. On the Laplace–Beltrami operator and brain surface flattening. IEEE Trans. Med. Imag. 18, 700–711.

Brechbühler, Ch., Gerig, G., Kübler, O., 1996. Parametrization of closed surfaces for 3-D shape description. CVGIP: Image Understand. 61, 154–170.

Cignoni, P., Montani, C., Scopigno, R., 1998. A comparison of mesh simplification algorithms. Comp. Graph. 22, 37–54.

Cignoni, P., Ganovelli, F., Montani, C., Scopigno, R., 2000. Reconstruction of topologically correct and adaptive trilinear isosurfaces. Comp. Graph. 24, 399–418.

Degener, P., Meseth, J., Klein, R., 2003. An adaptable surface parametrization method. In: Proceedings of the 12th International Meshing Roundtable, pp. 227–237.

Fischl, B., Sereno, M.I., Dale, A.M., 1999. Cortical surface-based analysis. II: Inflation, flattening, and a surface-based coordinate system. NeuroImage 9, 195–207.

Fischl, B., Liu, A., Dale, A.M., 2001. Automated manifold surgery: constructing geometrically accurate and topologically correct models of the human cerebral cortex. IEEE Trans. Med. Imag. 20, 70–80.

Floater, M.S., Hormann, K., 2005. Surface parameterization: a tutorial and survey. In: Dodgson, N.A., Floater, M.S., Sabin, M.A. (Eds.), Advances in Multiresolution for Geometric Modelling. Springer-Verlag, Berlin, pp. 157–186.

Funkhouser, T., Min, P., Kazhdan, M., Chen, J., Halderman, A., Dobkin, D., Jacobs, D., 2003. A search engine for 3D models. ACM Trans. Graph. 22, 83–105.

Garland, M., Heckbert, P.S., 1999. Optimal triangulation and quadric-based surface simplification. J. Comp. Geom. 14, 49–65.

Gerig, G., Styner, M., Shenton, M.E., Lieberman, J.A., 2001. Shape versus size: improved understanding of the morphology of brain structures. Shape versus size: improved understanding of the morphology of brain structures, MICCAI 2001. Lect. Notes Comp. Sci. 2208, 24–32.

Gu, X., Wang, Y., Chan, T.F., Thompson, P.M., Yau, S.T., 2004. Genus zero surface conformal mapping and its application to brain surface mapping. IEEE Trans. Med. Imag. 23, 949–958.

Gumhold, S., Borodin, P., Klein, R., 2003. Intersection free simplification. Int. J. Shape Mod. 9, 155–176.

Han, X., Xu, C., Braga-Neto, U., Prince, J.L., 2002. Topology correction in brain cortex segmentation using a multiscale, graph-based algorithm. IEEE Trans. Med. Imag. 21, 109–121.

Han, X., Xu, C., Prince, J.L., 2003. A topology preserving level set method for geometric deformable models. IEEE Trans. PAMI 25, 755–768.

Hormann, K., 2001. Theory and applications of parameterizing triangulations. Ph.D. thesis, Department of Computer Science, University of Erlangen.

Hurdal, M., Stephenson, K., 2004. Cortical cartography using the discrete conformal approach of circle packing. NeuroImage 23, S119–S128.

Ju, L., Hurdal, M.K., Stern, J., Rehm, K., Schaper, K., Rottenberg, D., 2005. Quantitative evaluation of three cortical surface flattening methods. NeuroImage 28, 869–880.

Kreyzsig, E., 1991. Differential Geometry. Dover, New York.

Kruggel, F., 2005. Techniques in analyzing the neocortial fine-structure. In: Leondes, C.T. (Ed.), Medical Imaging Systems, World Scientific Press, Singapore 5, pp. 255–279.

Kruggel, F., 2006. MRI-based volumetry of head compartments: normative values of healthy adults. NeuroImage 30, 1–11.

Park, J.Y., McInerney, T., Terzopoulos, D., Kim, M.H., 2001. A non-self-intersecting adaptive deformable surface for complex boundary extraction from volumetric images. Comp. Graph. 25, 421–440.

Pham, D.L., Prince, J.L., 1999. An adaptive fuzzy segmentation algorithm of magnetic resonance images. IEEE Trans. Med. Imag. 18, 737–752.

Pinkall, U., Polthier, K., 1993. Computing discrete minimal surfaces and their conjugates. Exp. Math. 2, 15–36.

Press, W.H., Teukolsky, S.A., Vetterling, W.T., Flannery, B.P., 1999. Numerical Recipes in C. Cambridge University Press, Cambridge, pp. 252–255.

Shattuck, D.W., Leahy, R.M., 2001. Graph based analysis and correction of cortical volume topology. IEEE Trans. Med. Imag. 20, 1167–1177.

Shen, L., Ford, J., Makedon, F., Saykin, A., 2004. A surface-based approach for classification of 3D neuroanatomic structures. Intel. Data Anal. 8, 519–542.

Tosun, D., Rettmann, M.E., Prince, J.L., 2004. Mapping techniuqes for aligning sulci across multiple brains. Med. Image Anal. 8, 295–309.

Toriwaki, J., Yonekura, T., 2002. Euler number and connectivity indexes of a three dimensional digital picture. Forma 17, 183–209.